Multidisciplinary Physicochemical Analysis of Oligothiophenes End-Capped by Nitriles: Electrochemistry, UV−Vis−Near-IR, IR, and Raman Spectroscopies and Quantum Chemistry

Juan Casado,[†] Rocío Ponce Ortiz,[†] Mari C. Ruiz Delgado,[†] Reiko Azumi,[‡] Richard T. Oakley,[§] Víctor Hernández,[†] and Juan T. López Navarrete*,[†]

Departamento de Química Física, Facultad de Ciencias, Universidad de Málaga, 29071 Málaga, Spain, Nanotechnology Research Institute, National Institute of Advanced Industrial Science and Technology, Tsukuba Central 5-2, Higashi 1-1-1, Tsukuba, Ibaraki 305-8565, Japan, and Department of Chemistry, University of Waterloo, Waterloo, Ontario N2L 3G1, Canada

Received: November 25, 2004; In Final Form: March 19, 2005

In this article, we investigate a series of α,ω-dicyano end-capped oligothiophenes $NC(C_4H_2S)_nCN$ ranging in length from the dimer to the hexamer ($n = 2-6$), in the neutral state as pure solids, by means of Fourier transform IR and Fourier transform Raman (FT-Raman) spectroscopies. The cyclic voltammetry analysis of the compounds in dichloromethane reveals that most of them show two oxidation and two reduction waves (i.e., a dual or amphoteric electrochemical behavior), associated with the injection of either positive or negative charges into the π-conjugated system. The doped species are characterized by in situ vis−near-IR and FT-Raman spectrochemistries. Density functional theory calculations have been also performed, at the B3LYP/6-31G** level, to assess information about the molecular geometries and vibrational features of the neutral and doped species and about the topologies of the molecular orbitals involved in the main electronic transitions that appear for the neutral forms in the visible spectral region and for the doped species in the near-IR region.

I. Introduction

Oligothiophenes have received great attention over the past few years for their potential use in a variety of devices, including nonlinear optics,[1] Schottky diodes,[2] organic light-emitting diodes (OLEDs),[3] and thin-film field-effect transistors (FETs).[4] The application of oligothiophenes in FETs is especially attractive, and there have been many efforts toward the improvement of the on−off ratio and the mobility. The most heavily studied oligomer has been α-sexithiophene (T_6H_2).[4a] Macroscopically, recent efforts to improve the FETs include the use of highly purified oligomers,[5] high-temperature film deposition,[6] single crystals,[7] etc., leading to better ordering of the molecules in the film and therefore improved transistor performance. At a molecular level, different chemical modifications have been proposed such as the use of alkyl side groups at the end α,ω-positions of oligothiophenes. This strategy has the twofold benefit of blocking these positions to further reactions, i.e., oxidation and polymerization, and of introducing ordering in the crystal. Very high mobility has been demonstrated when the terminal hydrogens of sexithiophene are replaced by *n*-hexyl groups.[8] Less success has been met with methyl,[4e,9] ethyl,[4d] and hexylthio[10] end-capping groups.

A particular attribute of importance for the use of oligothiophenes in many technological applications, which partially justifies the important place assumed by these oligomers in materials chemistry, is their ease of oxidation. Stable or very stable radical cations and higher oxidation states are formed at rather low potentials. In contrast, oligothiophenes are commonly quite difficult to reduce and do not form stable radical anions or dianions. This situation has been recently addressed by the synthesis of quinoid oligothiophenes,[11−13] such as a tetrahexylbis(dicyanomethylene)quaterthiophene analogue of 7,7,8,8-tetracyanoquinodimethane, which shows electrochemical reductions at very low cathodic potentials.[14] As aforementioned, redox amphoteric oligothiophenes are quite interesting for FET applications; hence one might visualize ambipolar FETs using a π-conjugated oligomer that could support the introduction of either negative or positive charges and in this way act as both a p-type and n-type semiconductor when properly polarized. This idea has been recently tested using an amphoteric quinoid terthiophene.[15a] Although no evidence for p-type conductivity was found in the first attempt, ambipolar behavior is finally reached for this quinoid system after proper optimizations of the film-forming conditions.[15b]

The fact that π-conjugated oligomers showing an amphoteric electrochemical behavior might find, by example, FET applications will depend on developing a detailed understanding of their structure, chemistry, and physicochemical properties. However, the attachment of suitable substituents at the end α,ω-positions of the π-conjugated backbone can be used to influence and perhaps control the solid-state structures of oligothiophenes. In this context, the crystal structures of a series of α,ω-dicyano end-capped oligothiophenes has been studied.[16] The authors chose the nitrile group as the substituent because it is assumed to be small enough to allow close intermolecular contacts in the solid state and additionally it is able to promote the ordering of oligothiophene chains through the development of intermolecular CN···H interactions. In fact, the well-ordered solid-state arrangement of these cyano-oligothiophenes constitutes a sig-

* Author to whom correspondence should be addressed. Phone: 34 952 213 18 65. Fax: 34-952-130-000. E-mail: teodomiro@uma.es.
[†] Universidad de Málaga.
[‡] National Institute of Advanced Industrial Science and Technology.
[§] University of Waterloo.

10.1021/jp0446175 CCC: $30.25
Published on Web 04/29/2005

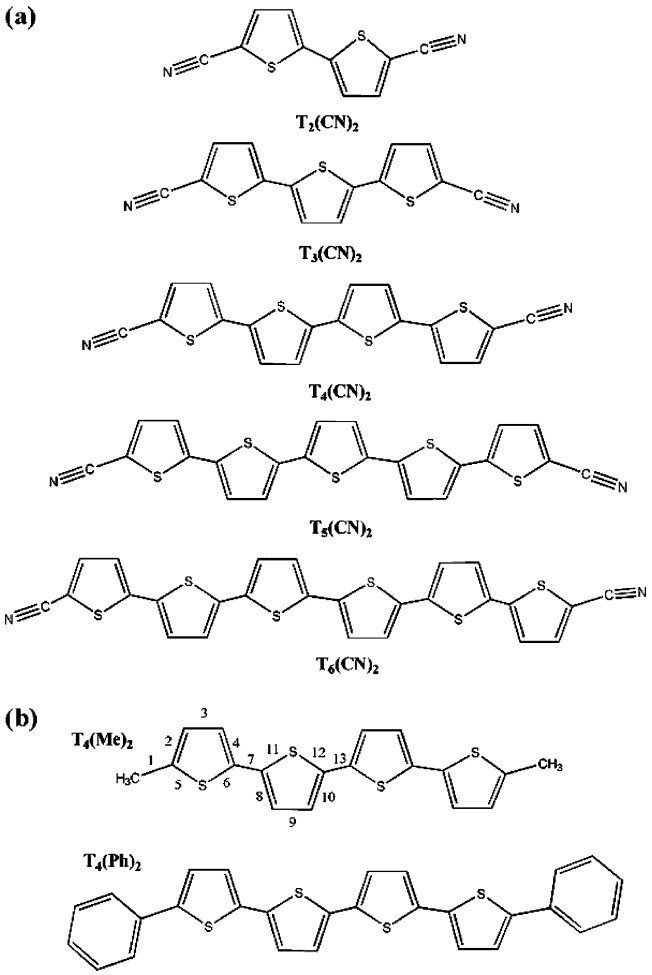

Figure 1. Structures and abbreviations of (a) the α,ω-dicyano end-capped oligothiophenes studied in this work and (b) two different end-capped quaterthiophenes (bond numberings are to be used in Table 3).

nificant improvement regarding the novel strategy of substitution of the α,ω- and β-thienyl positions with perfluorohexyl chains, which has been demonstrated to efficiently promote n-channel conduction in FETs.[15c] As a further study of these oligothiophenes end-capped by nitriles (Figure 1), in the present article we report on their redox properties and spectroscopic vibrational features. Using a combination of in situ spectrochemistry and quantum-chemical calculations, we document and explain several aspects of their chemistry such as their ease oxidation, the stability of their radical cations and dications, the formation of the radical anions and dianions upon reduction, and the main electronic absorptions for selected oxidation states and their relationship to other classes of oligothiophenes (interpreted in the light of time-dependent density functional theory (TD-DFT) calculations).

II. Results and Discussion

A. Optimized Geometries and Electronic Spectra of Neutral Compounds. Electronic absorption spectra of these systems have been previously reported and feature a strong absorption band in the visible spectral region, at around 400 nm, which progressively shifts to lower energies as the oligomeric chain grows up (namely, 338 nm in $T_2(CN)_2$, 382 nm in $T_3(CN)_2$, 416 nm in $T_4(CN)_2$, and 436 nm in $T_5(CN)_2$).[16] We also observed in all the cases a moderate positive solvatochromic shift, by 8 nm, with increasing solvent polarity (i.e., in passing from dichloromethane to dimethyl sulfoxide). Although the longer members of the series of chromophores do not show high solubility at room temperature, their spectral features are concentration-independent in the range examined, suggesting that the molecules do not aggregate.

TABLE 1: Optimized B3LYP/6-31G Values (in Å) for Selected Bond Lengths of the Neutral Forms of the $T_n(CN)_2$ Oligomers**

bond	$T_2(CN)_2$	$T_3(CN)_2$	$T_4(CN)_2$	$T_5(CN)_2$	$T_6(CN)_2$
$r(C_\alpha{=}C_\beta)$	1.381	1.382	1.382	1.383	1.383
$r(C_\beta{-}C_\beta)$	1.412	1.412	1.412	1.412	1.412
$r(C_\alpha{-}S)$[a]	1.750	1.755	1.756	1.757	1.758
$r(C_\alpha{-}C_{\alpha'})$	1.448	1.445	1.442	1.441	1.441
$r(C{\equiv}N)$	1.165	1.165	1.166	1.166	1.166
$r(C_\alpha{-}CN)$	1.415	1.414	1.414	1.413	1.413

[a] Innermost thienyl unit.

TABLE 2: Comparison between the Skeletal B3LYP/6-31G Bond Lengths (in Å) of $T_4(CN)_2$ and the Other Two Quaterthiophenes End-Capped by Methyl, $T_4(Me)_2$, and Phenyl, $T_4(Ph)_2$, Groups**

bond	$T_4(CN)_2$	$T_4(Ph)_2$	$T_4(Me)_2$
1	1.414	1.466	1.498
2	1.380	1.379	1.370
3	1.412	1.415	1.423
4	1.385	1.381	1.378
5	1.752	1.758	1.750
6	1.752	1.756	1.761
7	1.444	1.442	1.445
8	1.382	1.381	1.380
9	1.412	1.413	1.415
10	1.383	1.382	1.381
11	1.756	1.759	1.758
12	1.756	1.759	1.759
13	1.442	1.441	1.442

[a] Bond numbering refers to Figure 1.

To gain a deeper insight into the chain-length dependence of the molecular structure and equilibrium charge distribution of these α,ω-dicyano end-capped oligothiophenes, we have performed geometry optimizations, within the framework of the density functional theory, for the whole set of oligomers by using ab initio B3LYP/6-31G** model chemistry. (Table 1 summarizes a comparison between some representative skeletal bond lengths computed for the neutral forms of all the $T_n(CN)_2$ systems.) Although not reported in full detail, the B3LYP/6-31G** optimized geometries reveal that (i) the various thienyl units of a given compound display similar $C_\alpha{=}C_\beta$ and $C_\beta{-}C_\beta$ bond lengths, except for the two outermost $C_\alpha{=}C_\beta$ bonds of each chromophore, which are the shortest C=C double bond distance of the whole π-conjugated path, (ii) the $C_\alpha{-}S$ and interring $C_\alpha{-}C_{\alpha'}$ bonds become slightly shorter and longer, respectively, in going from the center of the oligomer toward its ends, and (iii) the $C_\alpha{-}CN$ bonds are predicted to shorten with increasing chain length of the oligothiophene. Table 2 additionally reports on the structural modifications induced by the attachment of three different types of α,ω-disubstituents (i.e., cyano, phenyl, or methyl) to a quaterthienyl spine. The greatest changes take place for the outermost thienyl units (i.e., those covalently linked to the end caps), whereas the geometry of the inner rings changes little from one compound to another.

For $T_2(CN)_2$, the mean single−double CC bond-length alternation (BLA) pattern of the thienyl rings directly linked to the cyano groups amounts to 0.0305 Å, whereas the corresponding values for the longer oligomers are 0.0300 Å for $T_3(CN)_2$ and 0.0295 Å for $T_4(CN)_2$, $T_5(CN)_2$, and $T_6(CN)_2$. These BLA values, related to the difference between the average lengths of single and double conjugated CC bonds, can be

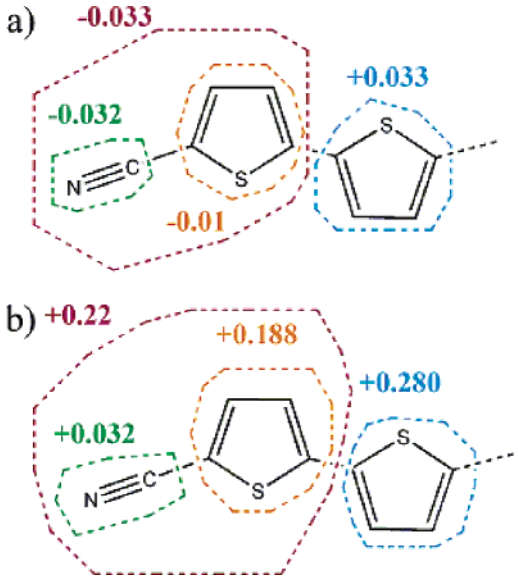

Figure 2. Overall summation (in *e*) of the B3LYP/6-31G** and UB3LYP/6-31G** natural population analysis (NPA) atomic charges on different molecular domains for (a) the neutral form and (b) the radical cation of $T_4(CN)_2$, taken as the prototypical case for the other $T_n(CN)_2$ oligomers.

compared with those of 0.0350 and 0.0490 Å obtained for $T_4(Ph)_2$ and $T_4(Me)_2$, respectively. Thus, B3LYP/6-31G** model chemistry reveals that the cyano disubstitution leads to a certain degree of quinoidization of the oligothienyl backbone, which saturates as the chain length becomes longer. This structural effect will be supported later by vibrational data.

Figure 2 reports the overall summation of the natural population analysis (NPA) atomic charges on different molecular domains, which can be hypothesized within the $T_4(CN)_2$ system in the neutral state as a prototypical case. B3LYP/6-31G** calculations show that the two outermost thienyl units of the chain are slightly charged negatively (namely, including in the summation the NPA charge on the CN group), while all the inner units are charged positively, as a consequence of the weak intramolecular charge transfer (ICT) taking place from the oligothienyl spine toward the electron-withdrawing nitrile end groups. The negative NPA charge over each CN group becomes larger with the molecular size, $-0.024e$ for $T_2(CN)_2$, $-0.029e$ for $T_3(CN)_2$, $-0.032e$ for $T_4(CN)_2$, $-0.033e$ for $T_5(CN)_2$, and $-0.034e$ for $T_6(CN)_2$, which is consistent with an increasing degree of ICT as the oligomer chain grows. We also observe that the NPA atomic charges on the C_α attached to the electron-deficient CN group and on its nearest sulfur atom greatly vary with respect to their counterparts in the inner rings. In this regard, the B3LYP/6-31G** NPA values for $T_5(CN)_2$ are $-0.348e$ and $0.511e$ for the outermost C_α and S atoms, respectively, as compared with $-0.230e$ and $0.465e$ for the central thiophene.

To provide insight into the UV−vis absorption spectra of the chromophores in the neutral state, TD-DFT calculations at the B3LYP/6-31G** level have been performed for all the systems. Transition energies, oscillator strengths, and highest occupied molecular orbital (HOMO)−lowest unoccupied molecular orbital (LUMO) gaps are listed in Table 3 along with the description of the experimental absorptions in terms of the main one-electron vertical excitations. Figure 3 sketches a diagram with the energies of the molecular orbitals around the gap within the series of compounds, whereas Figure 4 shows the topologies of the frontier molecular orbital (MO) of $T_2(CN)_2$ and $T_6(CN)_2$.

TABLE 3: TD-DFT//B3LYP/6-31G Vertical One-Electron Excitations (in eV) Related to the Strongest Visible Absorption of Each Neutral $T_n(CN)_2$ Oligomer in CH_2Cl_2**

compound	ΔE_{exp} (eV)	$\Delta E_{B3LYP/6-31G^{**}}$ (eV)	ΔE_{H-L} (eV)	description
$T_2(CN)_2$	3.67	3.53 ($f = 0.74$)	3.66	HOMO → LUMO
$T_3(CN)_2$	3.25	2.98 ($f = 1.14$)	3.14	HOMO → LUMO
$T_4(CN)_2$	2.98	2.65 ($f = 1.53$)	2.84	HOMO → LUMO
$T_5(CN)_2$	2.65	2.42 ($f = 1.90$)	2.64	HOMO → LUMO
$T_6(CN)_2$		2.27 ($f = 2.24$)	2.51	HOMO → LUMO

As reported in Table 3, the predictions of the TD-DFT calculations are in good agreement with the experimental data, and deviations between the measured and calculated excitation energies for the various electronic absorption bands recorded in the visible region (not shown) do not surpass 0.1−0.3 eV. As expected, the strongest absorption at around 400 nm is predominantly built up from the HOMO → LUMO excitation. Figure 4 shows that both frontier orbitals spread over the whole π-conjugated path, although the largest contributions to the HOMO of the longer oligomers come from the innermost thiophene rings. In the HOMO, the C═C bonds are π-bonding and have an alternating phase with respect to their adjacent C═C bonds, whereas in the LUMO the "C═C" units are π-antibonding and have the same phase as their neighbors.

From the schematic diagram showing the B3LYP/6-31G** energy levels around the band gap region (Figure 3), we learn that (i) the HOMO is rather less affected by the encapsulation of the π-conjugated backbone than the corresponding LUMO, since for the former frontier orbital the extension of the π-conjugated path toward the cyano groups is partially balanced by the negative inductive effect of the end caps, whereas the LUMO greatly varies in energy since both effects point in the same direction and (ii) from $T_2(CN)_2$ to $T_6(CN)_2$, both the HOMO and LUMO undergo an energy increase by ∼1.23 and ∼0.07 eV, respectively, because now the dominant effect is the overall conjugation of the system. As a result, a larger destabilization for the HOMO than for the LUMO occurs, which additionally leads to a steady reduction of the band gap (denoted as ΔE_{H-L} in Table 3).

It is worthy to mention that the energy of the vertical electronic transition from a doubly occupied MO to a vacant MO is predicted to be smaller than their energy gap, which might be ascribed to the reduced interelectronic interaction upon the single one-electron excitation (i.e., the interaction can be conceptually interpreted in a simply way as the balance between Coulomb and exchange terms, and expectedly it should decrease progressively with the increasing size of the π-conjugated system). Indeed, the DFT//B3LYP/6-31G** HOMO−LUMO gaps for the whole set of $T_n(CN)_2$ oligomers (ΔE_{H-L} in Table 3) are found to be always somewhat higher than the predicted TD-DFT//B3LYP/6-31G** energies for the corresponding HOMO−LUMO one-electron vertical excitations. The fact that the difference between the ΔE_{H-L} and $\Delta E_{B3LYP/6-31G^{**}}$ values is very little dependent on the molecular size (namely, it ranges from 0.13 eV in $T_2(CN)_2$ to 0.24 eV in $T_6(CN)_2$) indicates that the lowering of the HOMO−LUMO transition energy with increasing length of the π-conjugated chain is mainly determined by the narrowing of the HOMO−LUMO gap, more than to a significant difference in the energetic balance between the interelectronic interaction terms (i.e., Coulomb and exchange) from one oligomer to another.

The situation outlined in the preceding paragraphs must be stressed. First, despite being very frequently applied as a direct measure of the HOMO−LUMO gap and of the extent of π-conjugation of a system, UV−vis absorption spectra are not

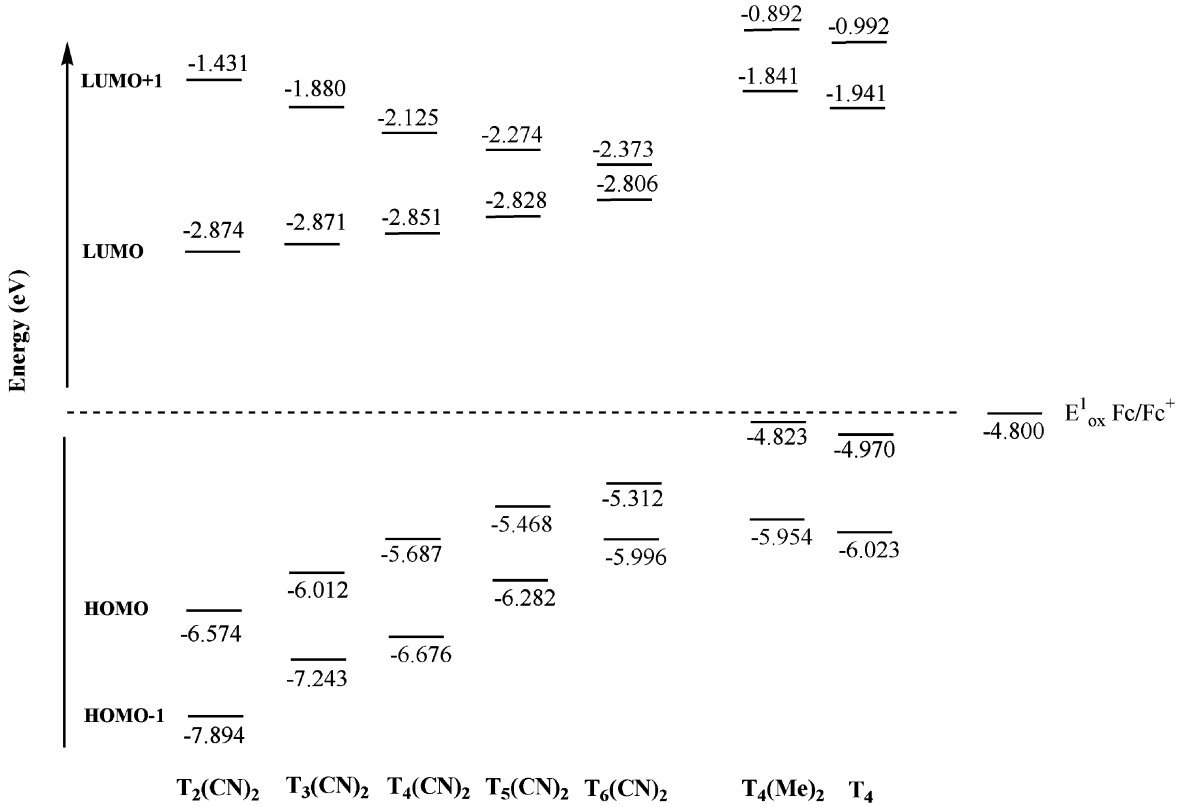

Figure 3. B3LYP/6-31G** one-electron energies (ϵ_i) diagram of the molecular orbitals around the band gap along the whole series of $T_n(CN)_2$ oligomers, unsubstituted quaterthiophene, and α,ω-dimethyl end-capped quaterthiophene.

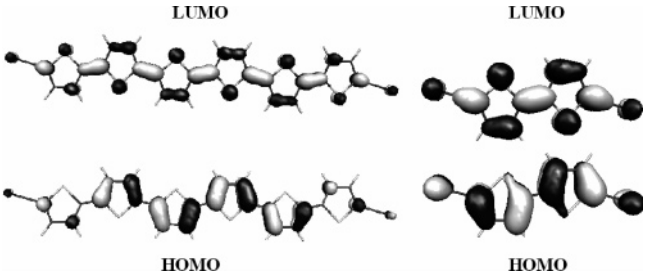

Figure 4. B3LYP/6-31G** electronic density contours (0.03*e*/bohr^3) for the frontier molecular orbitals of $T_2(CN)_2$ and $T_6(CN)_2$.

unambiguous in this use. It is frequent, when studying a homologous series of linear π-conjugated oligomers, that the optical properties reach saturation for quite short chain lengths, whereas the orbital energies still continue to change for longer oligomers. The Coulomb and exchange integrals are expected to decrease with increasing chain length (their trend of variation is in line with the assumption that in longer systems the electronic repulsion is smaller). However, the narrowing of the HOMO−LUMO gap with an increasing number of units in the π-conjugated chain is usually more pronounced (i.e., in our case of 1.15 eV from $T_2(CN)_2$ to $T_6(CN)_2$), so that the Coulomb and exchange terms play a minor role in determining the energy of the singlet excited state involved in the HOMO−LUMO excitation. As a conclusion, it is desirable that the analysis of the experimental UV−vis data would not be based on spectroscopic intuition only but guided by some accurate quantum-chemical calculation about the energies and topologies of the molecular orbitals, focusing on the usual multiconfigurational character of the different optical absorptions.

B. Cyclic Voltammetry. Previous works dealing with the electrochemical properties of several cyano-substituted oligothiophenes with short chain lengths (dimers or trimers) and various

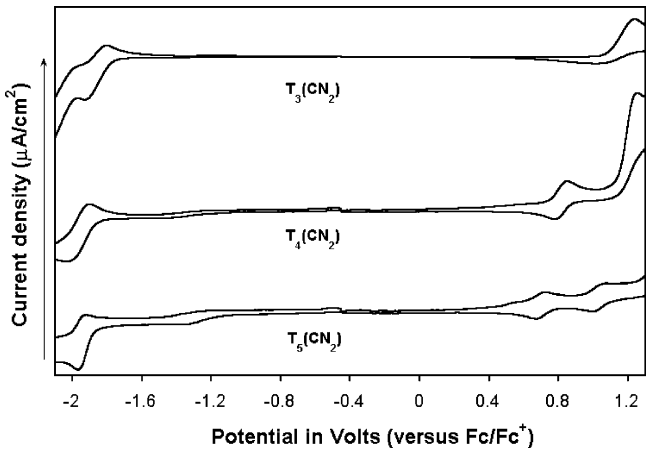

Figure 5. Cyclic voltammograms of the various $T_n(CN)_2$ oligomers.

substitution patterns can be found in the literature, mainly from Garnier and co-workers.[16−18] In the present article, we revisit their cyclic voltammetry (CV) waves from the new perspectives offered by the first-principle quantum-chemical calculations and in the light of the molecular point of view provided by the vibrational spectroscopic data. Furthermore, the electrochemical analysis is extended for the first time to the largest soluble members of the series of compounds (i.e., tetramer and pentamer). Figure 5 displays the CV of some selected $T_n(CN)_2$ oligomers, whereas Table 4 sums up the potential values recorded in the CV experiments.

It is well-known that nonfunctionalized oligothiophenes, ranging in length from 2 to 10 α-linked units, do not show cathodic processes at usually experimentally accessible electrochemical potentials. The strategy of introducing electron-acceptor groups, as nitrile moieties in our case, promotes the appearance of cathodic features, thus enriching the usual

TABLE 4: Potential Values for the Various Compounds (in V) versus Fc/Fc^+, as Measured in 0.1 M n-Bu_4NPF_6/CH_2Cl_2 Solution, with a Scan Rate of 100 mV s^{-1}, and Using Glassy Carbon as the Working Electrode, Pt Foil as the Counterelectrode, and an Ag/Ag^+ Electrode as a Pseudoreference[a]

peak notation[a]	$T_2(CN)_2$	$T_3(CN)_2$	$T_4(CN)_2$	$T_5(CN)_2$
E_{pr}^1(V)	−1.88	−1.94	−2.01	−1.99
E_{pr}^2(V)	−1.99	−2.18		
E_{pr}^3(V)	−2.22 (i)	−2.37 (i)		
E_{pa}^1(V)	1.31 (i)	1.06 (i)	0.78	0.66
E_{pa}^2(V)			1.15 (i)	1.04
E_{pa}^3(V)				1.41 (i)

[a] Irreversible processes are denoted as (i).

electrochemical behavior of these conjugated systems. As a result, the appearance of the first reversible reduction processes gives rise to the formation of anionic species, likely radical anions and dianions. As reported in Table 4, the corresponding electrochemical potentials (E_{pr}^1) progressively shift, although slightly, to more negative values upon chain-lengthening.

Assuming that the new incorporated electrons are accommodated into the empty LUMO, Koopman's theorem enables us to relate the absolute LUMO energies with the electrochemical potentials for the first reduction values. Since the absolute energy of the HOMO of ferrocene is theoretically estimated to be −4.800 eV (DFT//B3LYP/6-31G**) with respect to the vacuum level and given that the Fc/Fc^+ couple is our 0.000 V in the cyclic voltammetric experiments, it is possible to quantitatively afford theory/experiment comparisons. Theory nicely reproduces the magnitude and the evolution of the electrochemical reductions on increasing chain length; for example, E_{pr}^1 values for $T_3(CN)_2$ and $T_4(CN)_2$ are measured respectively at −1.940 and −2.010 eV, which compares with the calculated −1.930 and −1.950 eV values (the latter data are obtained as the difference between the energy of the HOMO of ferrocene and those of the LUMO of the oligomers). Qualitatively, one might think that the addition of new thiophene units (i.e., thus electron-enriching the central oligothienyl spine) progressively mitigates the electron-acceptor character of the nitriles, which should translate into the reduction of the electron affinity of the whole π-conjugated system. This can have some support on the orbital topologies of the LUMO, which undergo a continuous lack of weight by part of the atomic orbitals of the CN groups on going from the dimer to the hexamer (Figure 4).

To quantitatively illustrate the effects on the electrochemical response of the π-conjugated systems induced by the terminal encapsulation with opposite features, i.e., with inactive or weak electron donor end groups, the absolute energies of the frontier orbitals around the band gap for unsubstituted quaterthiophene and α,ω-dimethyl end-capped quaterthiophene are also included in Figure 3, together with the relevant data for the whole set of $T_n(CN)_2$ oligomers. Contrary to the α,ω-dicyano oligomers, the electron-enriched tetramer, $T_4(Me)_2$, does not show stable reduction processes, which is accounted for by the B3LYP/6-31G** calculations in the sense that its LUMO energy is much higher (by ∼1.0 eV) than that of its $T_4(CN)_2$ parent.[19] The scenario is however quite different for the anodic features that are shifted to lower energies in passing from the α,ω-dicyano to the α,ω-dimethyl encapsulation; thus, the potential value for the formation of the radical cation of $T_4(Me)_2$ is cathodically shifted by 0.73 V (0.05 V against the Fc/Fc^+ couple, in acetonitrile 0.1 M tetraethylammonium hexafluorophosphate[19]) from $T_4(CN)_2$, which is related to the stabilization of the HOMO by ∼0.8 eV from the former to the latter compound. One can observe in Figure 6 even a third irreversible oxidation process for $T_5(CN)_2$ that might be related to the generation of up to trications. However, $T_2(CN)_2$ and $T_3(CN)_2$ are not able to stabilize the radical cation, whereas the processes for the formation of the radical cation of $T_4(CN)_2$ and the monocation and dication of $T_5(CN)_2$ are reversible. Along the $T_n(CN)_2$ series, the homologue oxidation potentials shift to lower values upon chain-lengthening, which again is in accordance with the predictions of the DFT model chemistry. For instance, in the case of the first oxidation potentials, the trend of variation of the E_{pa}^1 values with the chain length is 1.31 V vs 1.77 eV for $T_2(CN)_2$, 1.06 V vs 1.21 eV for $T_3(CN)_2$, 0.78 V vs 0.89 eV for $T_4(CN)_2$, and 0.66 V vs 0.67 eV for $T_5(CN)_2$ (namely, the second reported value in each case refers to the difference between the absolute HOMO energies of ferrocene and the oligothiophene).

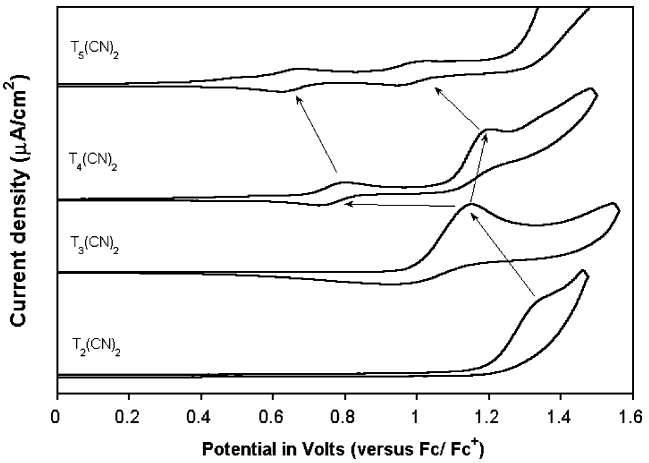

Figure 6. Detailed oxidative waves for the various $T_n(CN)_2$ oligomers.

In view of the topologies of the frontier molecular orbitals, one observes that the HOMO mainly spreads over the inner thienyl rings (i.e., particularly for the longest oligomers), so that it should be expected that the first oxidation potentials decrease almost linearly with the molecular size, because of the more efficient sharing of the positive charge in a more extended molecular domain. This reasoning however does not further hold for the generation of dications since it consists of the confinement of two positive charges in the middle part of the molecule. As a result, ΔE (i.e., the difference between the potentials for the generation of the radical cation and dication of a given oligomer) decreases on going from $T_3(CN)_2$ to $T_4(CN)_2$ but keeps almost the same value for $T_5(CN)_2$, which should be rationalized in terms of the nonlinear dependence of the repulsive electrostatic potential with distance. As for the dication, the charge confinement in the middle of the oligomer due to the presence of the nitrile end groups is well-addressed by indicating that ΔE for $T_4(Me)_2$ and $T_5(Me)_2$ amounts to 0.26 and 0.14 V, respectively, while the corresponding values for $T_4(CN)_2$ and $T_5(CN)_2$ are 0.42 and 0.37 V, respectively. This reveals the different mitigation of electrostatic repulsions between positive charges in both types of end-capped oligothiophenes.

C. Experimental and Theoretical Vibrational Spectra of Neutral Compounds. The Fourier transform Raman (FT-Raman) scattering spectra of the neutral forms of the $T_n(CN)_2$ oligothiophenes are shown in Figure 7. Figure 8 compares the Fourier transform IR (FT-IR) and FT-Raman spectral profiles of $T_2(CN)_2$, as the typical example for the other oligomers. However, Figure 9 displays a comparison between the experimental Raman profiles for $T_3(CN)_2$ as a pure solid and in CH_2-

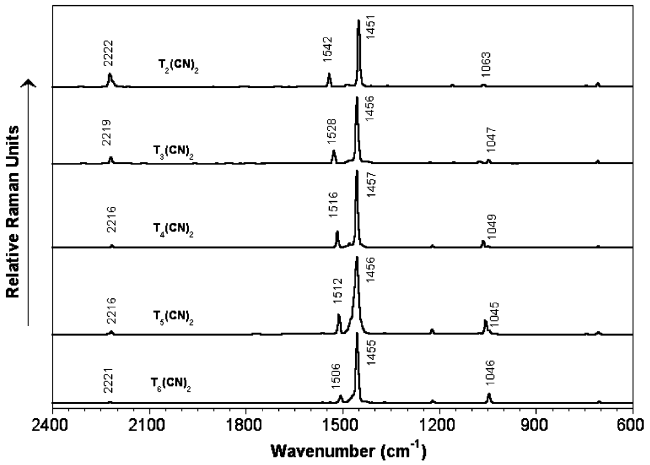

Figure 7. FT-Raman spectra of the $T_n(CN)_2$ oligomers in the neutral form (recorded on pure solids with a laser excitation wavelength of 1064 nm).

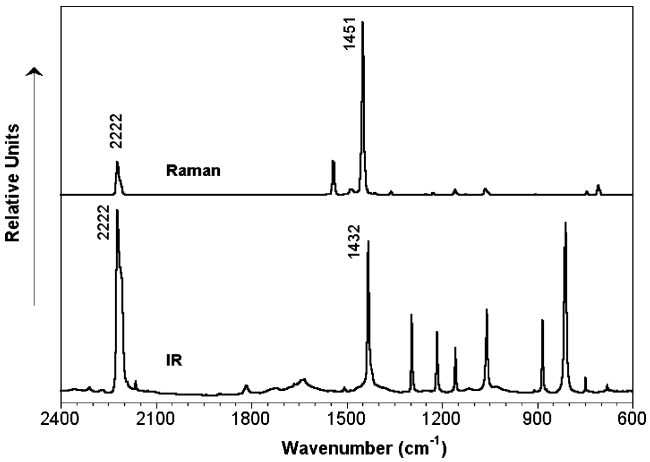

Figure 8. Comparison between the experimental FT-IR and FT-Raman spectra of $T_2(CN)_2$ in the 2400−600 cm^{-1} spectral range.

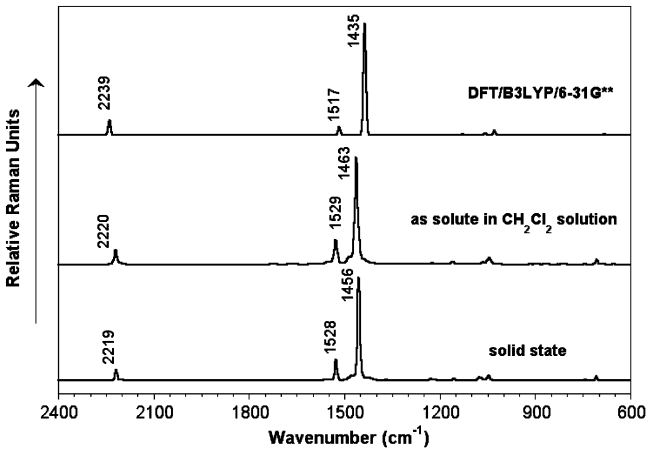

Figure 9. Comparison between the FT-Raman scattering profiles recorded for $T_3(CN)_2$ as a pure solid sample and upon CH_2Cl_2 solution (in the 2400−600 cm^{-1} spectral range) and the theoretical DFT// B3LYP/6-31G** one.

Cl_2 solution, together with its theoretical B3LYP/6-31G** spectrum. From the discovery of the electrically conducting polymers, vis−near-IR electronic absorption and infrared and Raman spectroscopies have been widely used to characterize many different types of π-conjugated systems (namely, oligomers and polymers), and among them Raman spectroscopy has been shown to be of great help in (i) estimating the degree of π-conjugation in neutral state along a homologous series of compounds with increasing chain lengths,[20−22] (ii) characterizing different types of conjugational defects induced by either chemical doping or photoexcitation,[23] and (iii) analyzing the efficiency of the intramolecular charge transfer in push−pull π-conjugated chromophores.[24−25]

TABLE 5: Evolution with the Chain Length of the Peak Positions of the Main Raman Features along the Whole Series of Neutral Oligomers.

$T_2(CN)_2$	$T_3(CN)_2$	$T_4(CN)_2$	$T_5(CN)_2$	$T_6(CN)_2$	description
2222	2219	2216	2216	2221	ν(C≡N)
1542(1533)	1528(1516)	1516(1508)	1512(1501)	1506(1497)	line A
1451(1441)	1456(1434)	1457(1431)	1456(1427)	1455(1423)	line B
1228	1229	1220	1222	1220	$\nu(C_\alpha-C_{\alpha'})$
	1077	1064	1055		δ(C−H)
1063	1047	1049	1045	1046	line D
708	708	708	706	706	ν(C−S)

[a] The B3LYP/6-31G** theoretical values are shown in parentheses.

The appearance of a few and overwhelmingly strong Raman features, even for systems with complex chemical structures, was satisfactorily accounted for by Zerbi and co-workers, through the now well-established effective conjugation coordinate (ECC) theory, assuming the existence of a collective C=C/C−C stretching mode strongly involved in the mechanism of the electron−phonon coupling characteristic of these one-dimensional π-conjugated systems.[26] In heteroaromatic poly-conjugated systems, the so-termed *collective ECC coordinate* has the analytical form of a linear combination of ring C=C/C−C stretchings, which points in the direction from a benzenoid structure (usually that of the ground state) to a quinonoid one (that corresponding to the electronically excited state). ECC theory states that the totally symmetric C=C/C−C stretching modes that describe the lattice dynamics of the ECC coordinate (namely, those which give rise to the few and rather strong Raman bands) undergo sizable dispersions both in frequency and intensity upon increasing conjugation length in the neutral systems. Thus, changes in Raman peak positions and relative intensities with increasing chain length are particularly useful in evaluating the mean conjugation length for each member of a given series of neutral oligomers. Furthermore, when these π-conjugated heteroaromatic oligothiophenes become oxidized (either chemically or electrochemically), various types of quinonoid-like charged defects are created.[27] This quinoidization also induces a significant red shift of the Raman lines associated with the π-conjugated path (due the softening of the C=C bonds), which is a marker of the type of charge defect created upon oxidation or reduction.[20−23]

Figure 8 shows again for these $T_n(CN)_2$ oligomers the usual simplicity of the FT-Raman scattering profiles as compared with their IR absorption spectra; the former display only three main features (i.e., near 2220, 1540, and 1450 cm^{-1}) associated to skeletal ν(CN) and ν(C=C) stretching vibrations, whereas for the latter a number of strong IR absorptions are still recorded below 1000 cm^{-1} (namely, most of them being due to out-of-plane γ(C−H) bending and γ_{ring} folding modes and consequently fully decoupled from the π-electron degree of freedom). Table 5 summarizes the evolution of the Raman peak frequencies upon chain-lengthening. By far, the strongest Raman band is measured near 1455 cm^{-1} while its associated eigenvector plotted in Figure 10 shows that this line arises from a oscillation of the whole alternating sequence of C=C/C−C bonds having the largest contributions from nuclear displacements of the central part of the chain. Moreover, along this vibration all π-conjugated C=C bonds lengthen in-phase while all π-conjugated C−C bonds shrink in-phase, so that it must be assigned to the *ECC* mode

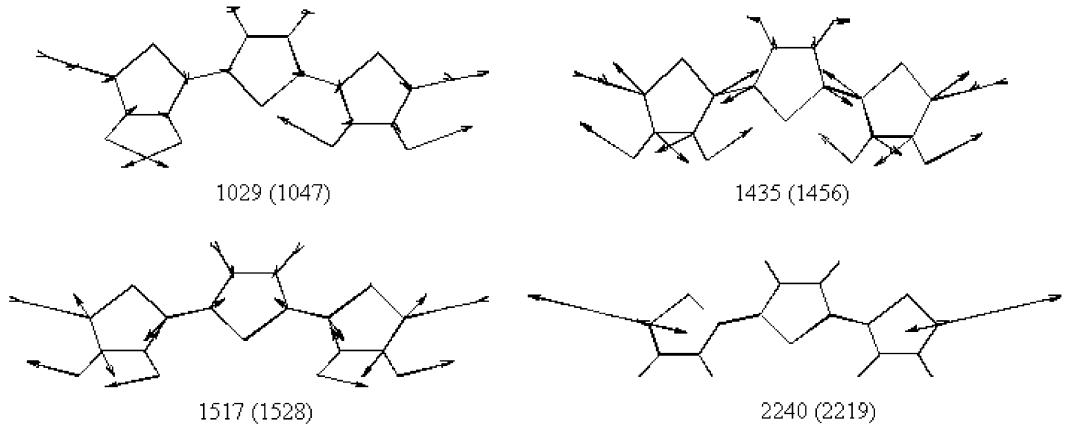

Figure 10. B3LYP/6-31G** vibrational eigenvectors associated with the most outstanding Raman features of neutral $T_3(CN)_2$. Theoretical and experimental (within parentheses) frequency values are given in cm^{-1}.

or *line B* in the terminology of α-linked oligothiophenes.[22,26] Its complementary *line A* appears at higher frequencies, and it is due to a ν(C═C/C─C), which is mainly located at the terminal rings of the oligothiophene chain.

B3LYP/6-31G** vibrational calculations of the Raman profiles have been performed for the whole set of compounds (namely, Table 5 summarizes the scaled wavenumbers for the characteristic Raman lines A and B of each chemical and Figures S1−S4 in the Supporting Information compare their experimental and theoretical profiles). Theoretical wavenumbers are always lower than experimental ones. The experimental chain-length downward dispersion observed for line A, by 36 cm^{-1}, from $T_2(CN)_2$ to $T_6(CN)_2$ is however nicely accounted for by DFT theory. Contrarily, whereas the peak position of line B is found to quickly reach saturation with chain lengths longer than the trimer, it is predicted to continuously downshift from the dimer to the hexamer. This discrepancy between theory and experiments might be ascribed to the usual tendency of B3LYP/6-31G** calculations to overestimate π-conjugation. Nonetheless, we also observe that the intensity of the Raman line B continues to increase relative to those of the ∼2215 cm^{-1} (ν(CN)) and ∼1515 cm^{-1} (line A) scatterings from $T_2(CN)_2$ to $T_6(CN)_2$. This selective enhancement of line B with increasing molecular size is however satisfactorily accounted for at the DFT// B3LYP/6-31G** level of theory. In this regard, it must be stressed that although calculations are performed in each case on a fully coplanar isolated entity in the vacuum and that X-ray diffraction data show some small conformation distortions out of the oligothienyl least-squares plane (particularly for the rings at both chain ends), Raman spectra collected for solutes change little with respect to those of the corresponding solids. It follows that overestimation of the peak position of the strongest Raman line B is not an artifact of the forced planarization but, in our opinion, an intrinsic deviation of the DFT//B3LYP/6-31G** methodology regarding the prediction of particular aspects of conjugational properties of these π-extended systems.

Lines A and B have important structural spectroscopic implications. For example, the BLA values reported in the preceding sections are always lower for the central rings than for the outermost ones, which agrees with the larger quinoidal character for this middle part of the molecule and with the statements of the ECC theory that foresee lower frequencies for the ν(C═C/C─C) Raman bands with increasing quinoidization or π-electron delocalization. Furthermore, it is observed that the peak position of line B changes moderately by 6 cm^{-1} within the series of compounds in accordance with the saturation of the BLA parameter for the central rings. However, the BLA data for the external thiophenes still continue to change for longer oligomers, which relates with the large downward dispersion of line A, namely, 36 cm^{-1} in going from $T_2(CN)_2$ to $T_6(CN)_2$.[24,25]

Let us now pay attention to the Raman bands near 2220 cm^{-1} due to the ν(CN) stretching vibrations. As reported in Table 5, which summarizes the evolution of the peak positions of the solid-state ν(CN) Raman bands along the whole set of oligomers, an initial red shift occurs in passing from the dimer to the tetramer followed by an upshift from the tetramer to the hexamer. It should be in principle expected for the ν(CN) Raman scatterings to appear at ever lower frequency values as the oligomer gets longer, due to the increasing easiness in attracting the π-electron cloud toward the electron-withdrawing cyano end groups, but this is not the current situation. The complete single-crystal structural characterization of the set of $T_n(CN)_2$ oligomers was achieved prior to this work.[16] The analysis of the X-ray diffraction data has revealed the main role played by the intermolecular interactions between nitrile groups in generating molecular ribbons in which the adjacent molecules are linked through close CN···H contacts. In addition, these CN···H interactions seem to be the driving force in determining the ribbon packing. Thus, for the trimer, tetramer, and pentamer, the ribbonlike arrays adopted slipped π-stack structures rather than the herringbone packing usually found in unsubstituted or α,ω-dialkyl end-capped terthiophene, quaterthiophene, sexithiophene, and octathiophene.[28] Only for the hexamer did the packing of the ribbons revert to the herringbone pattern.

We also observe that for the three shorter oligomers (namely, the longer ones are little or sparingly soluble) the ν(CN) Raman lines undergo a slight upshift when the pure vacuum-sublimated solids are dissolved in CH_2Cl_2, whereas they slightly downshift in dimethylsulfoxide (DMSO) solution. The upshift of the ν(CN) Raman scatterings from the pure solids to the CH_2Cl_2 solutions might account for the disappearance of the CN···H intermolecular interactions upon the complete loss of crystal order. However, the red shift of the ν(CN) peaks in passing from CH_2Cl_2 to a more polar solvent such as DMSO is in agreement (i.e., as in the case of the above-mentioned UV−vis absorption data) with an increased degree of ICT from the oligothienyl spine toward the two electron-withdrawing cyano end caps, so that the CN groups lose some triple-bond character. Nonetheless, as shown in Figure 9 for $T_3(CN)_2$, all the solutes display nearly the same Raman spectral profiles as the corresponding solids, which reinforces the fact that π-conjugation is the driving force that precludes large conformational distortions in solution from the nearly planar situation for the solids.

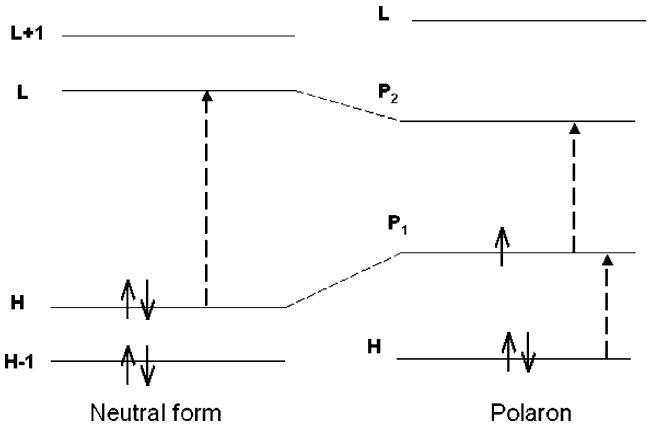

Figure 11. Schematic diagram showing the notation for the energy levels around the gap for a positively charged polaron in a π-conjugated system. The subgap energy levels and the new subgap optical transitions induced upon doping are denoted by bold lines and dashed arrows, respectively.

Additional spectroscopic evidence of the large involvement of the cyano end groups into the overall π-conjugation comes from the low frequency of the Raman-active ν(CN) stretching line along the series of oligomers (i.e., 2220−2215 cm^{-1}). These values are little higher than that found for a terthiophene-based quinodimethane in the solid state[29a] but nearly 45 cm^{-1} lower than that measured for a commercial sample of $CH_2(CN)_2$, (namely, a non-π-conjugated system).[29b]

D. In Situ Spectrochemistry and DFT Calculations of Doped Species. The UV−vis absorption spectra of $T_5(CN)_2$ recorded upon the slow addition of one equivalent of $FeCl_3$ or I_2 to a freshly prepared CH_2Cl_2 solution of the neutral oligomer show the appearance of two distinct absorptions at 583 and 1012 nm, which arise from subgap optical transitions (Figure 11), as is expected for a singly oxidized species [$T_5(CN)_2^{+\bullet}$]. Calculations with the TD-DFT formalism have been performed at the UB3LYP/6-31G** level to assign the above-mentioned absorption bands for the open-shell radical cationic species. Thus, the strongest feature at 2.25 eV is calculated at 2.13 eV with the largest oscillator strength ($f = 1.53$) and corresponds to a P1 → P2 monoelectronic promotion (Figure 11), while the low-energy band at 1.21 eV relates to the theoretical feature at 1.23 eV ($f = 0.21$) and may be assigned to a combined H → P1 + P1 → P2 double electronic promotion. This assignment of the two subgap absorptions of the radical cation deserves some further comments. TD-DFT//B3LYP/6-31G** calculations indicate that the mixing of the H → P1 and P1 → P2 vertical one-electron excitations is moderate, the CI coefficients being 0.34 (H → P1) and 0.80 (P1 → P2) for the band at higher energies and 0.84 (H → P1) and 0.57 (P1 → P2) for the second transition. Hence, the absorption at a shorter wavelength is assigned as due to the excitation of the unpaired electron (α-spin) from P1 to P2, whereas the band observed at longer wavelengths is due to the excitation of the β-spin from the HOMO to P1. However, the mixing between excited configurations is method-dependent since it depends on the reference wave function.

As usually found for many types of conjugated materials, the evolution from the neutral to the doped species induces significant bond-length modifications, leading to the attainment of an increased quinoid character as the number of removed π-electrons grows (see the predicted geometry changes between $T_4(CN)_2$ and $T_4(CN)_2^{+\bullet}$ in Figure 12). The degree of quinoidization can be quantified from the BLA values obtained for the various thiophene rings along the chain (i.e., evaluated as the

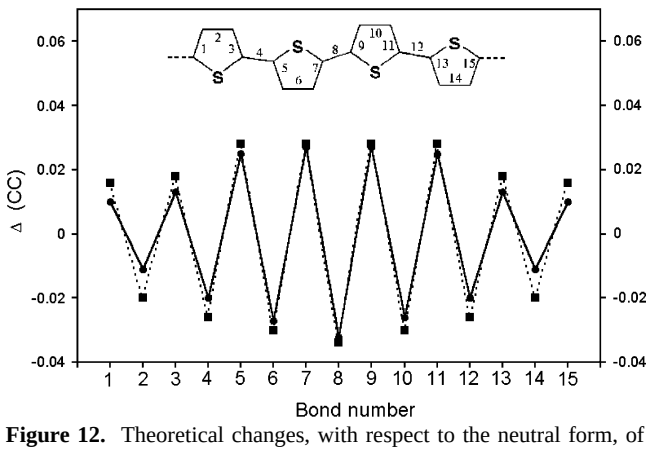

Figure 12. Theoretical changes, with respect to the neutral form, of the skeletal bond lengths of $T_4(CN)_2$ (circles) and $T_4(Me)_2$ (squares) upon the generation of the radical cation.

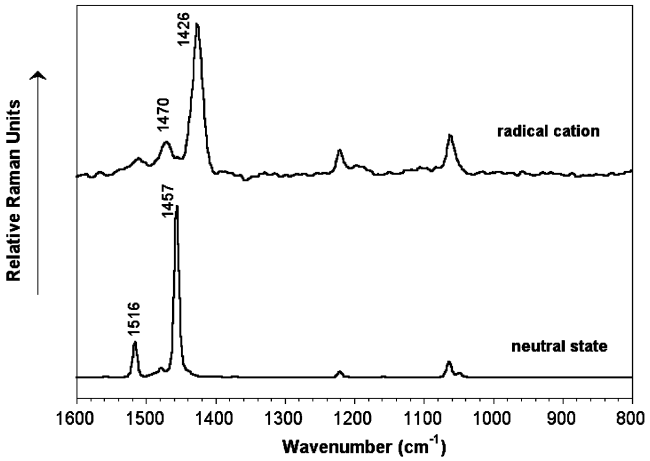

Figure 13. Evolution of the Raman spectrum of $T_4(CN)_2$, recorded as a thin film onto a quartz substrate, from the neutral state to the radical cationic species (i.e., the latter one was recorded just after exposure to dry iodine vapors in a drybox).

difference between the length of the $C_\beta C_\beta$ bond and the averaged value for the two $C_\alpha C_\beta$ bonds), 0.0295 Å for both the outer and inner thienyl units of neutral $T_4(CN)_2$, to be compared with the 0.007 and −0.022 Å from the ends toward the center of $T_4(CN)_2^{+\bullet}$. Thus, DFT model chemistry reveals a lengthening of the $C_\alpha C_\beta$ bonds and a shrinking of the $C_\alpha C_\alpha$ and $C_\beta C_\beta$ bonds in going from the neutral compound to the radical cation.

Regarding the electrostatic picture of the charged species derived from their equilibrium NPA atomic charge distributions, it is observed for the radical cation that each inner thienyl unit bears a partial positive charge of +0.280*e*, whereas the net charges over each outer thienyl ring end CN group amount to +0.188*e* and +0.032*e* (i.e., the central part of the tetramer stores nearly the 50% of the injected charge, and the percentage is expected to increase for longer oligomers). An opposite trend is predicted for the radical anion, for which the excess of charge is mainly accommodated around the CN groups, but the overall NPA charges on the inner rings are also computed to vary significantly with respect to the neutral form, likely due to the ICT toward the cyano groups so that the inner thienyl rings are poorer in π-electrons, in the pristine state, than in their unsubstituted parent oligothiophenes.

Let us finally derive further information from the evolution of the Raman spectral profile of the tetramer in going from the neutral state to the radical cation (Figure 13). After the removal of one electron, the strong Raman lines of $T_4(CN)_2$ at 1516 and 1457 cm^{-1} (i.e., those scatterings arising from the skeletal ν-

(C═C) vibrations mostly involved in the π-conjugation of the neutral compound) largely downshift to 1470 and 1426 cm^{-1}, respectively, in the case of $T_4(CN)_2^{+\bullet}$. Thus, the sizable dispersion upon oxidation of the characteristic Raman-active normal vibrations, usually termed as lines A and B, toward lower frequency values constitutes a measure of the degree of quinoidization of the π-conjugated path upon chemical doping, which is in agreement with the aforementioned picture derived from the changes of the BLA values between the neutral and doped species.

III. Summary and Conclusions

The strong impetus for improving the macroscopic parameters that determine the final implementation of oligothiophenes in microelectronic devices is justified. This whirlpool of works, however, also requires complementary analyses adopting molecular level perspectives. This work presents an analysis of the molecular scale structural and electronic properties of a family of oligothiophenes end-capped with electron-acceptor nitrile groups, which could be ideally visualized as candidates for ambipolar transport. The analysis is done by means of a selection of spectroscopic tools (namely, electron absorption and IR and Raman spectroscopies) whose data are carefully compared and combined with electrochemistry and supported by quantum chemistry. The study covers the case of the neutral and the charged species, in particular the radical cationic forms. This point is very important since semiconductor mobilities are but macroscopic transport of charges primarily injected into molecules.

The substitution with nitriles promotes the stabilization of cathodic processes that still appear at high electrochemical potentials for what might be desiderable for their applicability. This has been justified by the local affect, consisting of a small quinoidization, of the molecular properties of the oligothiophene chain, only significant in the terminal thiophenes. The local charge extraction toward the CN groups is balanced by the great capability of the thienyl spine to accommodate positive charges. In detriment, the anodic features are shifted to higher energies as is shown by the *pinning* of the structural relaxation associated with the generation of the radical cations in the central part of the molecules, far away of the competing electron-withdrawing nitriles. Upon oxidation, the more moderate peak change of the stronger Raman line (44 cm^{-1} for $T_4(CN)_2$ as compared with 65 cm^{-1} in $T_4(Me)_2$) is in agreement with the attainment of a quinoid structure in the conjugated path but more confined in the center. Theory nicely reproduces the inversion of the aromatic path to a quinoid one after electron extraction, in a similar extent that experiments suggest. Recently it has been shown that tetracyano methylene end capsulated oligothiophenes are ambipolar materials likely due to the full attainment of a quinoid structure of the oligothiophene chain. As a consequence, the slight affects on the whole chain by the nitrile encapsulation in the $T_n(CN)_2$ series, contrary to the whole attainment of a quinoid pattern in the tetracyano derivatives, outlines the way to improve at a molecular level the electric properties of oligothiophenes.

The chain-lengthening mitigates the whole effect of the terminal cyano groups, and the effect of the overall conjugation upon interaction of neighbor thiophene rings is dominant for the largest members of the series. In this sense, the molecular and spectroscopic data of the longer oligomers tend to reach the behavior of the nonsubstituted molecules, but it is not yet the case for our hexamer.

From a material science point of view, it is interesting to analyze the electrochemical band gap of a given molecular system showing an amphoteric redox behavior since this magnitude (potential window needed to be overcome for the injection of electrons and holes from an electrode) is directly related to the provided energy from a metallic junction of an electronic device (i.e., in field-effect transistors) in which ambipolar transport of charge is required. It is clear from this analysis that ambipolar transport always requires the presence of electron-acceptor groups attached to the oligothiophene backbone and that the electrochemical band gap can be effectively tuned through the control of the oligomer size.

IV. Experimental and Theoretical Details

FT-IR spectra were recorded on a Bruker Equinox 55 spectrometer. Compounds were ground to a powder and pressed in KBr pellets. FT-IR spectra, with a spectral resolution of 2 cm^{-1}, were collected over an average of 50 scans. Interference from atmospheric water vapor was minimized by purging the instrument with dry argon before starting the data collection. FT-Raman scattering spectra were collected on a Bruker FRA106/S apparatus with a Nd:YAG laser source ($\lambda_{exc} = 1064$ nm), in a backscattering configuration. The operating power for the exciting laser radiation was kept to 100 mW in all the experiments. Samples were analyzed as pure solids in sealed capillaries and dilute CH_2Cl_2 solutions (supplied by Aldrich with analytical grade). Typically, 1000 scans with 2 cm^{-1} spectral resolution were averaged to optimize the signal-to-noise ratio. UV−vis−near-IR absorption spectra were recorded either on a Lambda 19 Perkin-Elmer dispersive spectrophotometer or on an Agilent 8453 instrument equipped with a diode array for the fast recording of all the absorptions of the doped species appearing in the 190−1100 nm spectral region. Emission spectra were measured using a JASCO FP-750 spectrofluorometer interfaced to a Spectra Manager (v1.30.00) data station. No fluorescent contaminants were detected upon excitation in the wavelength region of experimental interest. Solutions were prepared with an absorbance between 0.1 and 0.2 at the excitation wavelength.

Cyclic voltammetry analysis was performed in CH_2Cl_2 solution (HPLC grade). Tetrabutylammonium hexafluorphosphate (0.1 M as supporting electrolyte) was purchased from Fluka and used as received, without further purification. Solutions were deaerated by N_2 bubbling prior to each measurement, which also were run under a continuous N_2 gas flow. Electrochemical experiments were performed in a two-compartment cell equipped with a glassy carbon working microelectrode ($\varnothing = 1$ mm) and a platinum wire counter electrode. An Ag/AgCl electrode was used as a reference, which was checked against ferrocene/ferricinium couple (Fc/Fc^+) before and after each experiment. Electrochemical experiments were carried out with a Voltalab 40 potentiostat from Radiometer Copenhagen with positive feedback compensation.

DFT calculations were carried out by means of the Gaussian 98 program[30] running on SGI Origin 2000 supercomputer. We used the Becke's three-parameter exchange functional combined with the LYP correlation functional (B3LYP).[31] It has already been shown that the B3LYP functional yields similar geometries for medium-sized molecules as MP2 calculations do with the same basis sets.[32,33] Moreover, the DFT force fields calculated using the B3LYP functional yield infrared spectra in very good agreement with experiments.[34,35] We also made use of the standard 6-31G* basis set.[36] Optimal geometries were determined on isolated entities. From the resulting ground-state optimized geometries, harmonic vibrational frequencies and

infrared intensities were calculated analytically, whereas Raman intensities where calculated numerically with the B3LYP functional.

We used the often-practiced adjustment of the theoretical force fields in which calculated harmonic vibrational frequencies are uniformly scaled down by a factor of 0.96 for the 6-31G** calculations, as recommended by Scott and Radom.[33] This scaling procedure is often accurate enough to disentangle serious experimental misassignments. All quoted vibrational frequencies reported along the paper are thus scaled values. The theoretical spectra were obtaining by convoluting the scaled frequencies with Gaussian functions (10 cm^{-1} width at the half-height). The relative heights of the Gaussians were determined from the theoretical Raman-scattering activities.

Vertical electronic excitation energies were computed by using the TD-DFT approach.[37,38] The 12 lowest-energy electronic excited states were at least computed for all the molecules. The computational cost of TD-DFT is roughly comparable to that of single-excitation theories based on a Hartree−Fock (HF) ground state, such as single-excitation configuration interactions (CIS). Numerical applications reported so far indicate that TD-DFT formalism employing current exchange-correlation functionals performs significantly better than HF-based single-excitation theories for the low-lying valence excited states of both closed-shell and open-shell molecules.[39] TD-DFT calculations were carried out using the B3LYP functional and the 6-31G** basis set on the previously optimized molecular geometries obtained at the same level of calculation.

Radical anions and cations were treated as open-shell systems and were computed using spin-unrestricted UB3LYP wave functions. The maximun value obtained for S^2 was 0.76, very close to the 0.75 theoretically expected for a doublet, showing that spin contamination is almost absent.

Acknowledgment. In honor of Professor Rafael Suau on the occasion of his 60th birthday. J.C. thanks the Ministerio de Ciencia y Tecnología for a "Ramón y Cajal" position of chemistry at the University of Málaga. The authors acknowledge the Dirección General de Enseñanza Superior, Ministerio de Educación y Ciencia, Spain, for support of this investigation through projects BQU2000-1156 and BQU2003-03194. The research has also been supported by the Junta de Andalucía, Spain, under grant FQM-0159. M.C.R.D. and R.P.O. are also grateful to the Ministerio de Educación y Ciencia and the Junta de Andalucía, respectively, for their personal grants.

Supporting Information Available: Comparisons between the DFT//B3LYP/6-31G** theoretical and experimental Raman profiles of $T_2(CN)_2$, $T_4(CN)_2$, $T_5(CN)_2$, and $T_6(CN)_2$. This material is available free of charge via the Internet at http://pubs.acs.org.

References and Notes

(1) (a) Zhao, M.-T.; Singh, B. P.; Prasad, P. N. *J. Chem. Phys.* **1988**, *89*, 5535. (b) Thienpont, H.; Rikken, G. L. J. A.; Meijer, E. W.; ten Hoeve, W.; Wynberg, H. *Phys. Rev. Lett.* **1990**, *65*, 2141. (c) Wada, T.; Wang, L. Fichou, D.; Higuchi, H.; Ojima, J.; Sasabe, H. *Mol. Cryst. Liq. Cryst. Sci. Technol., Sect. A* **1994**, *255*, 149.

(2) Fichou, D.; Horowitz, G.; Nishikitani, Y.; Garnier, F. *Chemtronics* **1988**, *3*, 176. (b) Fichou, D.; Horowitz, G.; Nishikitani, Y.; Roncali, J.; Garnier, F. *Synth. Met.* **1989**, *28*, C729. (c) de Leeuw, D. M.; Lous, E. J. *Synth. Met.* **1994**, *65*, 45.

(3) (a) Geiger, F.; Stoldt, M.; Schweizer, H.; Bäuerle, P.; Umbach, E. *Adv. Mater.* **1993**, *5*, 922. (b) Uchiyama, K.; Akimichi, H.; Hotta, S.; Noge, H.; Sakaki, H. *Mater Res. Soc. Symp. Proc.* **1994**, *328*, 389.

(4) (a) Horowitz, G.; Fichou, D.; Peng, X.; Xu, Z.; Garnier, F. *Solid State Commun.* **1989**, *72*, 381. (b) Horowitz, G.; Peng, X.; Fichou, D.; Garnier, F. *J. Appl. Phys.* **1990**, *67*, 528. (c) Paloheimo, J.; Kuivalainen, P.; Stubb, H.; Vuorimaa, E.; Yli-Lahti, P. *Appl. Phys. Lett.* **1990**, *56*, 1157. (d) Akimichi, H.; Waragai, K.; Hotta, S.; Kano, H.; Sasaki, H. *Appl. Phys. Lett.* **1991**, *58*, 1500. (e) Waragai, K.; Akimichi, H.; Hotta, S.; Kano, H.; Sasaki, H. *Synth. Met.* **1993**, *55*−*57*, 4053. (f) Garnier, F.; Hajlaoui, R.; Yassar, A.; Srivastava, P. *Science* **1994**, *265*, 1684. (g) Dodabalapur, A.; Katz, H. E.; Torsi, L.; Haddon, R. C. *Science* **1995**, *269*, 1560.

(5) Katz, H. E.; Torsi, L.; Dodabalapur, A. *Chem. Mater.* **1995**, *7*, 2235.

(6) Servet, B.; Horowitz, G.; Ries, S.; Lagorsse, O.; Alnot, P.; Yassar, A.; Deloffre, F.; Srivastava, P.; Hajlaoui, R.; Lang, P.; Garnier, F. *Chem. Mater.* **1994**, *6*, 1809.

(7) Horowitz, G.; Garnier, F.; Yassar, A.; Hajlaoui, R.; Kouki, F. *Adv. Mater.* **1996**, *8*, 52.

(8) Garnier, F.; Yassar, A.; Hajlaoui, R.; Horowitz, G.; Deloffre, F.; Servet, B.; Ries, S.; Alnot, P. *J. Am. Chem. Soc.* **1993**, *115*, 8716.

(9) Waragai, K.; Akimichi, H.; Hotta, S.; Kano, H.; Sakaki, H. *Phys. Rev. B* **1995**, *52*, 1786.

(10) Katz, H. E.; Dodabalapur, A.; Torsi, L.; Elder, D. *Chem. Mater.* **1995**, *7*, 2238.

(11) Yui, K.; Aso, Y.; Otsubo, T.; Ogura, B. *Bull. Chem. Soc. Jpn.* **1989**, *62*, 1539.

(12) (a) Higuchi, H.; Yoshida, S.; Uraki, Y.; Ojima, J. *Bull. Chem. Soc. Jpn.* **1998**, *71*, 2229. (b) Hernandez, V.; Calvo Losada, S.; Casado, J.; Higuchi, H.; Lopez Navarrete, J. T. *J. Phys. Chem. A* **2000**, *104*, 661.

(13) Higuchi, H.; Nakayama, T.; Koyama, H.; Ojima, J.; Wada, T.; Sasabe, H. *Bull. Chem. Soc. Jpn.* **1995**, *68*, 2363.

(14) Casado, J.; Miller, L. L.; Mann, K. R.; Pappenfus, T.; Higuchi, H.; Ortí, E.; Milián, B.; Pou-Amérigo, R.; Hernandez, V.; Lopez Navarrete, J. T. *J. Am. Chem. Soc.* **2002**, *124*, 12380.

(15) (a) Pappenfus, T. M.; Chesterfield, R. J.; Frisbie, C. D.; Casado, J.; Raff, J. D.; Miller, L. L.; Mann, K. R. *J. Am. Chem. Soc.* **2002**, *124*, 4184. (b) Chesterfield, R. J.; Newman, C. R.; Pappenfus, T. M.; Ewbank, P. C.; Haukaas, M. H.; Mann, K. R.; Miller, L. L.; Frisbie, C. D. *Adv. Mater.* **2003**, *15*, 1278. (c) Facchetti, A.; Yoon, M.-H.; Stern, C. L.; Katz, H. E.; Marks, T. J. *Angew. Chem., Int. Ed.* **2003**, *42*, 3900. (d) Facchetti, A.; Yoon, M.-H.; Stern, C. L.; Hutchison, G. R.; Ratner, M. A.; Marks, T. J. *J. Am. Chem. Soc.* **2004**, *126*, 13480. (e) Facchetti, A.; Mushrush, M.; Yoon, M.-H.; Hutchison, G. R.; Ratner, M. A.; Marks, T. J. *J. Am. Chem. Soc.* **2004**, *126*, 13859.

(16) Barclay, T. M.; Cordes, A. W.; MacKinnon, C. D.; Oakley, R. T.; Reed, R. W. *Chem. Mater.* **1997**, *9*, 981.

(17) Hapiot, P.; Demanze, F.; Yassar, A.; Garnier, F. *J. Phys. Chem.* **1996**, *100*, 8397 and references therein.

(18) Demanze, F.; Godillot, P.; Garnier, F.; Hapiot, P. *J. Electroanal. Chem.* **1996**, *414*, 61.

(19) Zotti, G.; Schiavon, G.; Berlin, A., Pagani, G. *Chem. Mater.* **1993**, *5*, 430 and 620.

(20) Sakamoto, A.; Furukawa, Y.; Tasumi, M. *J. Phys. Chem.* **1994**, *98*, 4635.

(21) (a) Yokonuma, N.; Furukawa, Y.; Tasumi, M.; Kuroda, M.; Nakayama, J. *Chem. Phys. Lett.* **1996**, *255*, 431. (b) Harada, I.; Furukawa, Y. In *Vibrational Spectra and Structure*; Durig, J., Ed.; Elsevier: Amsterdam, 1991; Vol. 19, p 369.

(22) (a) Hernandez, V.; Casado, J.; Ramirez, F. J.; Zotti, G.; Hotta, S.; Lopez Navarrete, J. T. *J. Chem. Phys.* **1996**, *104*, 9271. (b) Casado, J.; Otero, T. F.; Hotta, S.; Hernandez, V.; Ramírez, F. J.; Lopez Navarrete, J. T. *Opt. Mater.* **1998**, *9*, 82. (c) Moreno Castro, C.; Ruiz Delgado, M. C.; Hernandez, V.; Hotta, S.; Casado, J.; Lopez Navarrete, J. T. *J. Chem. Phys.* **2002**, *116*, 10419. (d) Moreno Castro, C.; Ruiz Delgado, M. C.; Hernandez, V.; Shirota, Y.; Casado, J.; Lopez Navarrete, J. T. *J. Phys. Chem. B* **2002**, *106*, 7163.

(23) (a) Casado, J.; Hernandez, V.; Hotta, S.; Lopez Navarrete, J. T. *J. Chem. Phys.* **1998**, *109*, 10419. (b) Casado, J.; Hernandez, V.; Hotta, S.; Lopez Navarrete, J. T. *Adv. Mater.* **1998**, *10*, 1258. (c) Casado, J.; Miller, L. L.; Mann, K. R.; Pappenfus, T. M.; Kanemitsu, Y.; Orti, E.; Viruela, P. M.; Pou-Amerigo, P.; Hernandez, V.; Lopez Navarrete, J. T. *J. Phys. Chem. B* **2002**, *106*, 3872. (d) Casado, J.; Miller, L. L.; Mann, K. R.; Pappenfus, T. M.; Hernandez, V.; Lopez Navarrete, J. T. *J. Phys. Chem. B* **2002**, *106*, 3597. (e) Casado, J.; Ruiz Delgado, M. C.; Shirota, Y.; Hernandez, V.; Lopez Navarrete, J. T. *J. Phys. Chem. B* **2003**, *107*, 2637.

(24) (a) Hernandez, V.; Casado, J.; Effenberger, F.; Lopez Navarrete, J. T. *J. Chem. Phys.* **2000**, *112*, 5105. (b) Casado, J.; Hernandez, V.; Kim, O.-K.; Lehn, J.-M.; Lopez Navarrete, J. T.; Delgado Ledesma, S.; Ponce Ortiz, R.; Ruiz Delgado, M. C.; Vida, Y.; Perez-Inestrosa, E. *Chem.—Eur. J.* **2004**, *10*, 3805.

(25) (a) Gonzalez, M.; Segura, J. L.; Seoane, C.; Martin, N.; Garin, J.; Orduna, J.; Alcala, R.; Villacampa, B.; Hernandez, V.; Lopez Navarrete, J. T. *J. Org. Chem.* **2001**, *66*, 8872. (b) Casado, J.; Pappenfus, T. M.; Miller, L. L.; Mann, K. R.; Orti, E.; Viruela, P. M.; Pou-Amerigo, P.; Hernandez, V.; Lopez Navarrete, J. T. *J. Am. Chem. Soc.* **2003**, *125*, 2534.

(26) (a) Zerbi, G.; Castiglioni, C.; Del Zoppo, M. *Electronic Materials: The Oligomer Approach*; Wiley-VCH: Weinheim, 1998; p 345. (b) Castiglioni, C.; Gussoni, M.; Lopez Navarrete, J. T.; Zerbi, G. *Solid State*

Commun. **1988**, *65*, 625. (c) Lopez Navarrete, J. T.; Zerbi, G. *J. Chem. Phys.* **1991**, *94*, 957 and 965 (d) Hernandez, V.; Castiglioni, C.; Del Zoppo, M.; Zerbi, G. *Phys. Rev. B* **1994**, *50*, 9815. (e) Agosti, E.; Rivola, M.; Hernandez, V.; Del Zoppo, M.; Zerbi, G. *Synth. Met.* **1999**, *100*, 101. (f) Zerbi, G. *Handbook of Conducting Polymers*; Marcel Dekker: New York, 1998.

(27) (a) Ehrendorfer, Ch.; Karpfen, A. *J. Phys. Chem*. **1994**, *98*, 7492. (b) Ehrendorfer, Ch.; Karpfen, A. *J. Phys. Chem.* **1995**, *99*, 5341.

(28) Fichou, D. *J. Mater. Chem.* **2000**, *10*, 571 and references therein.

(29) (a) Ruiz Delgado, M. C.; Hernandez V.; Casado J.; Lopez Navarrete J. T. Raimundo J.-M.; Blanchard, P.; Roncali, J. *Chem.—Eur. J.* **2003**, *9*, 3670. (b) Casado, J.; Pappenfus, T. M.; Mann K. R.; Milián, B.; Hernandez V.; Casado J.; Lopez Navarrete J. T. *ChemPhysChem* **2004**, *5*, 529.

(30) Frisch, M. J.; Trucks, G. W.; Schlegel, H. B.; Scuseria, G. E.; Robb, M. A.; Cheeseman, J. R.; Zakrzewski, V. G.; Montgomery, J. A., Jr.; Stratmann, R. E.; Burant, J. C.; Dapprich, S.; Millam, J. M.; Daniels, A. D.; Kudin, K. N.; Strain, M. C.; Farkas, O.; Tomasi, J.; Barone, V.; Cossi, M.; Cammi, R.; Mennucci, B.; Pomelli, C.; Adamo, C.; Clifford, S.; Ochterski, J.; Petersson, G. A.; Ayala, P. Y.; Cui, Q.; Morokuma, K.; Malick, D. K.; Rabuck, A. D.; Raghavachari, K.; Foresman, J. B.; Cioslowski, J.; Ortiz, J. V.; Stefanov, B. B.; Liu, G.; Liashenko, A.; Piskorz, P.; Komaromi, I.; Gomperts, R.; Martin, R. L.; Fox, D. J.; Keith, T.; Al-Laham, M. A.; Peng, C. Y.; Nanayakkara, A.; Gonzalez, C.; Challacombe, M.; Gill, P. M. W.; Johnson, B. G.; Chen, W.; Wong, M. W.; Andres, J. L.; Head-Gordon, M.; Replogle, E. S.; Pople, J. A. *Gaussian 98*, revision A.7; Gaussian, Inc.: Pittsburgh, PA, 1998.

(31) Becke, A. D. *J. Chem. Phys.* **1993**, *98*, 1372.

(32) Stephens, P. J.; Devlin, F. J.; Chabalowski, F. C. F.; Frisch, M. J. *J. Phys. Chem.* **1994**, *98*, 11623.

(33) Novoa, J. J.; Sosa, C. *J. Phys. Chem.* **1995**, *99*, 15837.

(34) Scott, A. P.; Radom, L. *J. Phys. Chem.* **1996**, *100*, 16502.

(35) Rauhut, G.; Pulay, P. *J. Phys. Chem.* **1995**, *99*, 3093.

(36) Francl, M. M.; Pietro, W. J.; Hehre, W. J.; Binkley, J. S.; Gordon, M. S.; Defrees, D. J.; Pople, J. A. *J. Chem. Phys.* **1982**, *77*, 3654.

(37) Runge, E..; Gross, E. K. U. *Phys. Rev. Lett.* **1984**, *52*, 997. Gross, E. K. U.; Kohn, W. *Adv. Quantum Chem.* **1990**, *21*, 255. Gross, E. K. U.; Ullrich, C. A.; Gossman, U. J. In *Density Functional Theory*; Gross, E. K. U., Driezler, R. M., Eds. Plenum Press: New York, 1995; p 149.

(38) Casida, M. E. In *Recent Advances in Density Functional Methods*; Chong, D. P., Ed.; World Scientific: Singapore, 1995; Part 1, p 115.

(39) Koch, W.; Holthausen, M. C. *A Chemist's Guide to Density Functional Theory*; Wiley-VCH: Weinheim, 2000.